Available online at www.sciencedirect.com

ScienceDirect

Geochimica et Cosmochimica Acta 290 (2020) 408–423

Geochimica et Cosmochimica Acta

www.elsevier.com/locate/gca

Validation and calibration of soil δ^2H and brGDGTs along (E-W) and strike (N-S) of the Himalayan climatic gradient

Iris van der Veen [a,*], Francien Peterse [b], Jesse Davenport [c], Bernd Meese [a], Bodo Bookhagen [a], Christian France-Lanord [c], Ansgar Kahmen [d], Hima J. Hassenruck–Gudipati [f], Ananta Gajurel [g], Manfred R. Strecker [a], Dirk Sachse [e]

[a] *Universität Potsdam, Institut für Erd- und Umweltwissenschaften, Potsdam-Golm, Germany*
[b] *Department of Earth Sciences, Utrecht University, the Netherlands*
[c] *Geochemistry, Centre des Recherche Petrographiques et Geochimiques (CNRS-CRPG), Vandœuvre-lés-Nancy, France*
[d] *University of Basel, Botanical Research, Basel, Switzerland*
[e] *GFZ German Research Centre for Geosciences, Section 5.1: Geomorphology, Organic Surface Geochemistry Lab, Potsdam, Germany*
[f] *Department of Geological Sciences, The University of Texas at Austin, 2275 Speedway, M.S. C9000, Austin, TX 78712, USA*
[g] *Tribhuvan University, Tri-Chandra College, Central Department of Geology, Kathmandu, Nepal*

Received 18 February 2019; accepted in revised form 12 September 2020; available online 22 September 2020

Abstract

Reconstructing the timing of mountain range uplift and the evolution of high-altitude plateaus is important when attempting to understand potential feedbacks between tectonics and climate at geological timescales. This requires proxies that are able to accurately reconstruct elevation during different time periods in the past. Often, the sensitivity of climatic parameters to elevation gradients, recorded in geological archives such as soils, is used to estimate paleoelevations. However, most proxies reflect an indirect response to elevation change, adding uncertainties to reconstructions. In this study, we aim to identify those sources of uncertainty with respect to elevation reconstructions and test if the combined application of two such proxies, i.e., stable isotopes (δ^2H) of plant waxes in modern soils and surface waters and bacterial membrane lipids (brGDGTs) in soils, which can potentially reduce uncertainties in the estimation of (paleo-) elevation. We performed this study in four Himalayan catchments (from west to east: Sutlej, Alaknanda, Khudi, and Arun), of which each individual catchment is subject to a unique precipitation regime, relative influences of moisture sources, and vegetation cover. In total, we analyzed 275 surface water samples, 9 precipitation samples, 131 xylem water samples, and 60 soil samples, which were collected between 2009 and 2014.

The following key observations were made: Soil nC_{31}-alkane δ^2H values (δ^2H_{wax}) in the Sutlej, Alaknanda, Khudi, and Arun generally record surface water δ^2H values, confirming that the first-order control on the plant wax isotopic signature is precipitation δ^2H and, therefore, the elevation in orogenic settings. We identified aridity as the factor that introduces scatter to this relationship. BrGDGT-derived Mean Annual Temperature (MAT) correlates in a statistically significant manner with sample site elevation and a 14-year annual average of remotely sensed land-surface temperature, showing that the main process influencing the brGDGT distribution is the adiabatic cooling of air.

In an effort to combine these proxies to improve uncertainties in elevation reconstruction, elevations were inferred from both the δ^2H_{wax} and brGDGT distributions. Arid, high elevation sites appear to underestimate actual sample site elevations using δ^2H values while sites subject to high (>23–25 °C) annual temperatures overestimate the actual sample site elevation using brGDGT distributions. Elevations inferred from both proxies under such paleoclimatic conditions should be interpreted

* Corresponding author.
E-mail address: Veen@geo.uni-potsdam.de (I. van der Veen).

https://doi.org/10.1016/j.gca.2020.09.014

with caution. Elevations derived from the brGDGT distribution appear to most accurately reconstruct elevation. However, we show that the difference in elevation between the two proxies, described by the proposed $\Delta_{Elevation}$ parameter, can provide information on the hydrological conditions of the soil's depositional environment. In conclusion, we emphasize that knowledge of the sample site's climatic conditions are essential to reconstruct elevation from paleoarchives. In particular, knowledge of moisture availability and annual air temperatures are important, as these have been found to cause the largest scatter in the observed data.

Keywords: Alkanes; δ^2H; GDGT; Satellite imagery; Paleoelevation; Himalaya; Soil

1. INTRODUCTION

The uplift of mountain ranges has been a key interest in climate and tectonic studies due to its impact on atmospheric circulation patterns, erosion, and precipitation patterns (Zhisheng et al., 2001; Clift et al., 2008). For example, the uplift of the Himalayan mountain range has played a key role in the onset and intensification of the Indian (ISM) and East Asian (EASM) monsoons, as well as in changing the global carbon cycle due to increasing weathering of freshly exposed bedrock (Dettman et al., 2003; Molnar and England, 1990; Quade et al., 2007; Poulsen et al., 2010; Garzione et al., 2000a). Testing these scenarios, uplift histories, and comparison with coeval climatic records are needed.

To reconstruct mountain range paleoelevation, we use proxies that record the persistent hydrological and climatological gradients preserved in geological archives. These proxies include numerous stable isotope and lipid biomarker approaches, such as $\delta^{18}O$ in pedogenic carbonates (Garzione et al., 2000b; Quade et al., 2007), leaf wax δ^2H (Zhuang et al., 2014; Bai et al., 2015; Peterse et al., 2009; Polissar et al., 2009; Jia et al., 2008), and branched tetraether membrane lipid distributions (Ernst et al., 2013; Wang et al., 2017; Sinninghe Damsté et al., 2008). These aforementioned proxies are all based on climatic parameters that are observed to co-vary with elevation, and hence indirectly record elevation. Rayleigh distillation processes during rainout result in a negative relationship between the isotopic composition ($\delta^{18}O$ and δ^2H) of precipitation and elevation (Dansgaard, 1964; Gat et al., 2000). Temperature generally decreases with increasing elevation. The δ^2H values in *n*-alkanes derived from higher terrestrial plants have shown a strong relationship with mean precipitation δ^2H values, which have been used for paleohydrological and paleoelevation reconstruction (Sauer et al., 2001; Huang et al., 2004; Sachse et al., 2004; Smith and Freeman, 2006; Hou et al., 2008). The potential of leaf wax δ^2H to record elevation has initially been shown at Mt Gongga in China (Jia et al., 2008) and later at Mt Shennongjia, Mt. Wuyi and Mt Tianshan (Luo et al., 2011), and Mt Meghalaya (Ernst et al., 2013). These studies reflect that soil δ^2H_{wax} records overall δ^2H from precipitation, and thus indirectly records the elevation.

Even though $\delta^{18}O$ and δ^2H values in precipitation primarily correlate with elevation, locally or seasonally varying processes and climatic conditions, such as heterogenic precipitation patterns, complex topography, and the relative influence of multiple moisture sources, can distort the general linear elevation relationships (e.g. Rohrmann et al., 2014; Hren et al., 2009; Galewsky, 2009).

Similarly, mean annual air temperature (MAT) generally decreases with elevation due to the adiabatic cooling of air, and is therefore also an indirect measure of elevation. This temperature change can be reflected by distributional changes in branched glycerol dialkyl glycerol tetraethers (brGDGTs) (Weijers et al., 2007). BrGDGTs are membrane lipids produced by soil bacteria, which vary in the number (4–6) of methyl branches attached to their alkyl backbone, the position of these methyl branches (5 or 6 position), and the number (0–2) of internal cyclizations, depending on the MAT and pH of the soil in which they are produced (Weijers et al., 2007; De Jonge et al., 2014b). As such, MAT can be reconstructed based on the molecular signature of brGDGTs in an environmental sample (Weijers et al., 2007; De Jonge et al., 2014a; Naafs et al., 2017). The ability of brGDGTs to track adiabatic cooling was first illustrated in a study at Mt Kilimanjaro, where a good relation was found between brGDGT-derived MAT and altitude (Sinninghe Damsté et al., 2008). Subsequently, good relations between brGDGT signals and MAT were found along the southeastern margin of the Tibetan Plateau (Wang et al., 2017), Mt Gongga (Peterse et al., 2009), and Mt Meghalaya (Ernst et al., 2013), among others. Outside of East Asia, this relationship has also been found in the Andes (Nieto-Moreno et al., 2016) and Africa (Coffinet et al., 2014, 2017; Jaeschke et al., 2018).

Nevertheless, the latest global temperature transfer functions still contain a substantial amount of scatter, indicating that the brGDGT temperature proxy is influenced by additional climatic parameters, such as soil moisture content (SMC) and precipitation amount/aridity (Peterse et al., 2012; Dirghangi et al., 2013; Menges et al., 2014; Wang et al., 2014; Dang et al., 2016; Naafs et al., 2017), but possibly also by soil and vegetation type (Davtian et al., 2016) and the co-occurrence of brGDGT-producing microbial communities with distinct temperature relationships (De Jonge et al., 2019; Dearing Crampton-Flood et al., 2020). These effects can introduce uncertainties in the relationship between brGDGT signals and temperature, and thus the proxy's robustness in recording elevation.

To assess possible sources of scatter in the individual relations of soil *n*-alkane δ^2H and brGDGTs with elevation, and thus the suitability of these proxies in paleoelevation reconstructions, both proxies were applied in parallel at several altitudinal transects. This revealed, for example,

that the rain belt surrounding Mt Kilimanjaro likely disturbed the relation between soil *n*-alkane δ^2H and elevation due to a D-depletion in the precipitation and consequently in the soil *n*-alkanes (Peterse et al., 2009; Zech et al., 2015). A similar spatial heterogeneity in precipitation was shown at Mt Kenya and Mt Rungwe, resulting in weak or absent relationships between the soil *n*-alkane δ^2H and elevation (Coffinet et al., 2017). Nevertheless, the combined application of brGDGTs and soil *n*-alkane δ^2H in the Andes, Mt Meghalaya, and the Southern Alps in New Zealand did show the expected orography effect on temperature and precipitation (Nieto-Moreno et al., 2016; Ernst et al., 2013; Zhuang et al., 2014).

In this study, we further validate the individual relations of brGDGT-derived MAT and δ^2H_{wax} with altitude using a combination of field and remote-sensing data. In a second step, the proxies are combined and we investigate whether this combination reduces potential uncertainties in the elevation estimates. Specifically, we analyze the stable isotopic composition (δ^2H) of surface waters, xylem waters (i.e. the lipid H source), and long chain n-alkanes, as well as brGDGT signals in modern soils along four altitudinal gradients along the Himalayan orogeny. These altitudinal transects are subject to varying precipitation regimes, different degrees of aridity, relative influences of moisture sources, and vegetation cover, which allows a thorough investigation of the impact that different environmental factors have on δ^2H_{wax} and brGDGTs. Combining the multi-proxy data with satellite-derived climate products, we aim to identify the controlling secondary factors that potentially alter the relationship between source water δ^2H and δ^2H_{wax}, as well as physically measured MAT and brGDGT-derived MAT. Ultimately, we discuss how the offset between these parameters can potentially impact paleoelevation studies and the interpretation of these proxies in sedimentary archives.

2. STUDY AREA

The Himalayan mountain range separates the Tibetan Plateau from the Indian subcontinent, traversing 2700 km along the range from the Karakoram in Pakistan in the northwest through India, Nepal, and Bhutan into the Arunachal Pradesh in the southeast. The range varies in width between ~400 km in the west and ~150 km in the east, containing several significant mountain peaks.

The Himalayan range acts as an orographic barrier separating the humid regions in the foreland and arid sections in the rain shadow, resulting in varying precipitation patterns along the Southern Himalayan Front (SHF). Two partly independent, but interfering climatic circulation systems dominate the precipitation regime in the Himalaya: the Indian Summer Monsoon (ISM) system and the Western Disturbances (WD) (Bookhagen and Burbank, 2010; Cannon et al., 2014). The ISM moves along the SHF and transports moisture from the Bay of Bengal toward the northeast, causing heavy rainfall along the southern slopes of the mountain front during summer (Bookhagen et al., 2005). The second major moisture source is the WD, originating from the Caspian, Black, and Mediterranean seas, transporting winter precipitation between December and March (Cannon et al., 2014; Wulf et al., 2010; Dash et al., 2009). Spatially, the dominance of the ISM decreases from east to west, whereas the WD becomes particularly influential west of 78°E (Bookhagen and Burbank, 2010). The Himalayan range creates an extreme gradient between the humid tropical climate in the foreland and alpine conditions at higher elevations. The two major climatic gradients that strongly influence the vegetation cover and type along the orogen are the decreasing air temperature from low to high elevations and the decreasing amount of moisture from east to west (Singh and Singh, 1987).

3. METHODS

3.1. Elevation transects

Four transects from the northeast to the southwest were selected in the Sutlej, Alaknanda, Khudi Khola (hereafter referred to as Khudi), and Arun catchments, of which the first two are located in the western Himalaya in India and the latter two in central and eastern Nepal (Fig. 1). These four transects each cover a large altitudinal gradient and consequently also span large ranges in precipitation, vegetation, and temperature (Fig. 2).

The Sutlej catchment elevation transect ranges from 475 to 3533 m over a horizontal distance of ~170 km. The lower sites (<3000 m asl) receive 1500–2000 mm rainfall annually (cf. TRMM 2B31, Bookhagen and Burbank, 2010), decreasing to <500 mm/year at the higher sample sites (>3000 m asl) (Fig. 2A). Mean Annual Temperature (MAT) in the catchment ranges between 9.7 °C and 25.4 °C, with an average of 19.7 °C (2000–2014 yearly average, MOD11C3, Wan and Hulley, 2015; Wulf et al., 2016). Concurrently, with the decrease in rainfall amount and the increase in elevation, the Enhanced Vegetation Index (EVI) shows that vegetation cover in the catchment decreases with elevation (Fig. 2A).

The Alaknanda catchment transect ranges from 346 to 3155 m with a horizontal distance of 160 km. Annual rainfall varies between 300 and 2600 mm/year and consists of two rainout belts (at ~500 and ~2000 m, Fig. 2B) due to a two-step rise in relief (Fig. 2B), as described in Bookhagen and Burbank (2006). The 14-year average MAT in the catchment is 19.8 °C, ranging between 7.1 °C and 26.8 °C (Wan and Hulley, 2015).

The Khudi, where the transect ranges from 2155 to 4085 m asl with a horizontal transect of ~13 km, receives rainfall amounts of >3900 mm/year (Fig. 2C). There is little variation in the amount of rainfall along the altitudinal transect due to its short distance. MAT varies between 7.5 °C and 19.5 °C with an average temperature of 13.1 °C.

The transect in the Arun valley ranges from 225 to 2580 m over a horizontal transect of 160 km. Annual rainfall amounts along the transect vary between 2000 and 4000 mm/year (Fig. 2D), showing a two-belt rainout pattern similar to the Alaknanda transect (at ~500 and ~2000 m, Fig. 2D). MAT varies between 3.5 °C and 26.7 °C, with an average of 16.3 °C.

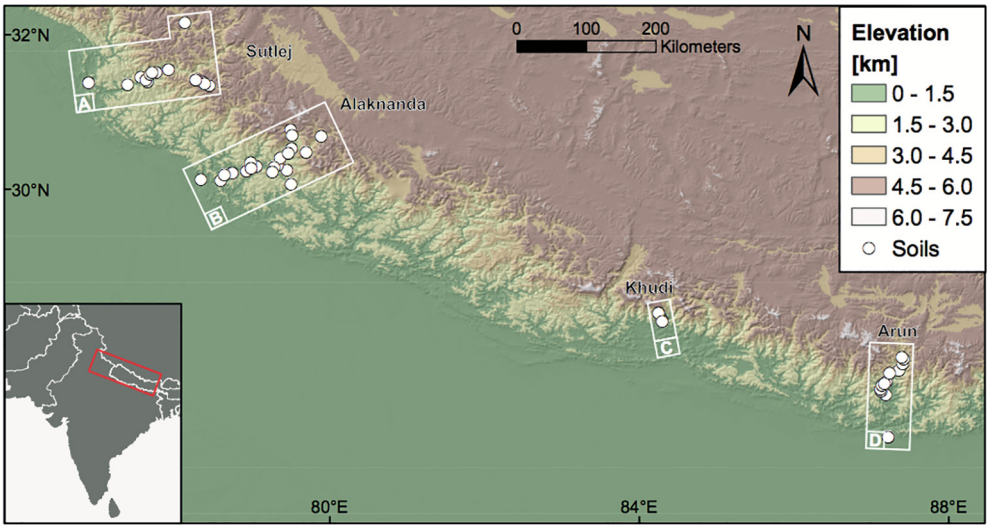

Fig. 1. Topographic overview of the Himalaya (SRTM V3). White circles indicate the sample sites of the soils along four altitudinal gradients. White rectangles indicate areas over which the swath profiles were determined, and labeling corresponds to the swath profiles shown in Fig. 2.

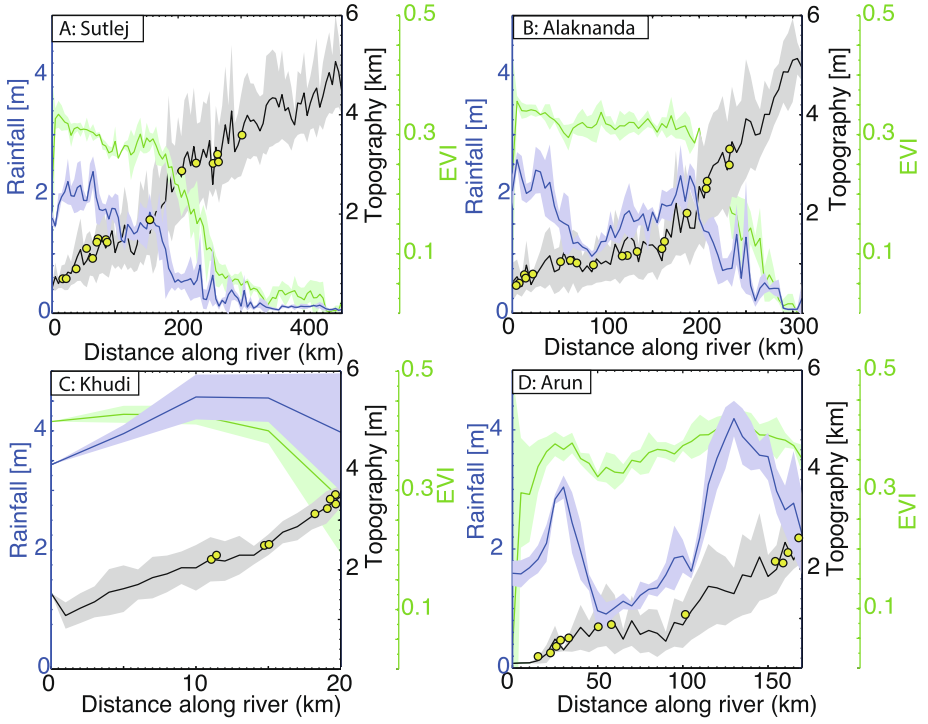

Fig. 2. 10-km wide swath profiles along the four altitudinal transects in the Himalaya (cf. Fig. 1). 12-year average JJA mean TRMM 2B31 precipitation in blue (Bookhagen and Burbank, 2010), 17-year average (2000–2017) MODIS derived EVI in green (Didan, 2015), and topography in black with 1-sigma standard deviation (gray) (USGS, 2006). Yellow circles indicate soil sample sites along the elevation transects. (For interpretation of the references to colour in this figure legend, the reader is referred to the web version of this article.)

3.2. Sample collection

Soil (0–5 cm, without litter) and water samples in the Alaknanda and the Sutlej catchment were obtained in September/October 2014, whereas soils and water in the Arun catchment were collected both in September 2011 and October/November 2012 (Hoffmann et al., 2016). In the Khudi Khola catchment, only soils were sampled at various depths in September 2009.

All soils were sampled adjacent to roads/paths in the catchments, which were checked for undisturbed soils. Soils were never sampled on steep slopes, but from the most horizontal part of the terrain. However, due to the generally steep terrain in the study area it is possible that geomorphic

processes (e.g. creep and downslope transport) have transported material from higher elevations.

In total, 107 water samples and 17 soil samples in the Sutlej catchment, 52 water samples and 21 soil samples in the Alaknanda catchment, 10 soil samples in the Khudi Khola catchment, and 116 water samples and 12 soil samples in the Arun catchment were collected. In addition, 35 xylem water samples from dominating vegetation at sample sites in the Alaknanda, 33 in the Arun, and 63 in the Sutlej catchments were collected. At every xylem water sampling location, 9 branches were collected from 3 individuals of the same species. Per sample location, the 2 most dominant angiosperm species were sampled. Due to the large climatic gradient, it was not possible to sample the same species along the entire elevation transect. After collecting the branches, the bark was removed to prevent mixing between xylem water and phloem water, after which the peeled branches were placed in airtight containers. Xylem waters were extracted at a vacuum line at the university of Basel (Newberry et al., 2017). Extracted xylem water was measured on a TCEA-IRMS for $\delta^{18}O$ and $\delta^{2}H$ values. For the Khudi precipitation samples, rain gauges were installed at three stations allowing daily collection of rainwater in 2013 (time series data for the Ghalegaon station (IAEA). These stations are at Ghalegaon village (2103 m) on the western crest of the basin and two near the Khudi river at the Khudi Hydropower Intake station (968 m) and Probi village (1456 m). At higher elevations between 2500 and 4050 m, cumulated rain waters were collected over long periods in sealed 40 liter plastic containers (DRUM) surmounted with a 15 cm funnel.

3.3. Analysis of $\delta^{2}H$ and $\delta^{18}O$ values of water samples

The surface water $\delta^{2}H$ and $\delta^{18}O$ values sampled in the Alaknanda and Sutlej catchment were measured on a Picarro Cavity Ringdown Spectrometer L2140-I at GFZ Potsdam, with a precision of 0.08‰ for $\delta^{18}O$ and 0.5‰ for $\delta^{2}H$. For the Khudi precipitation samples, waters were analysed at CRPG laboratory (Nancy-France) using a Eurovector-Isoprime EA-IR-MS coupled with a chromium reactor. Samples were systematically repeated three times and external reproducibility was better than ±1‰. Samples were analysed with internal standards every five samples and calibrated using the V-SMOW, GISP, and V-SLAP standards. All samples were filtered through a 0.45 µm syringe and stored in 2 mL vials. The samples were injected 10 times, with a volume of 1 µl, and the first three injections were discarded for each individual sample, to avoid any memory effects. The measurements were normalized using a two-point correction using VSMOW2 and SLAP2 standards, provided by the IAEA.

The stable isotope composition is reported using the δ-notation relative to the Vienna Standard Mean Ocean Water (VSMOW) standard as:

$$\delta\ [‰] = \left(\frac{R_{Sample}}{R_{Standard}} - 1\right), \quad (1)$$

where R is the ratio of heavy isotopes relative to light isotopes ($^{18}O/^{16}O$ and $^{2}H/^{1}H$). All values are reported in per mille ‰ (implying a factor of 1000).

3.4. Lipid extraction

The soil samples were freeze-dried and stored in precombusted (500 °C) glass vials. Before extraction, all soil samples were sieved with a 2 mm sieve, and any leaves and large roots were removed to avoid any contamination from modern organic material. A total lipid extract (TLE) was extracted from the soil samples using an Accelerated Solvent Extractor (ASE) (Type Dionex ASE 350) using 9:1 dichloromethane:methanol as a solvent. Samples were initially separated into two fractions using columns containing 1.5–2 gram of precombusted silica gel. Samples were added to the top of the column, and then rinsed with 12 mL of hexane to obtain the hydrocarbon fraction. The GDGT fraction was obtained by subsequent rinsing with 1:1 dichloromethane:methanol.

3.5. Lipid analysis

The hydrocarbon fraction containing the *n*-alkanes was analysed on an Agilent GC MSD (Agilent 5975C MSD, Agilent 7890A GC with Agilent J&W HP-5 MS column, 30 m × 0.25 m × 0.25 µm film) coupled to an FID. A Thermo Scientific Delta V Plus IRMS coupled to a Trace 1310 GC (Agilent GC MSD (RESTEK, Rtx-5 Crossbond ms column, 30 m × 0.25 mm × 0.25 µm df. 5% diphenyl, 95% dimethyl polysiloxane) via an Isolink pyrolysis furnace operated at 1420 °C was used at Potsdam University for the measurement of the *n*-alkane $\delta^{2}H$ values ($\delta^{2}H_{wax}$). The H_3^+ factor was determined at the beginning of every sequence, and was constant (3.9 ± 0.7) throughout the entire duration of the measurements, indicating stable conditions in the ion source. All samples were measured in duplicates, with a standard deviation of <3‰, and a C_{10}–C_{40} standard measured in between every 10 samples. The $\delta^{2}H_{wax}$ values were all normalized to the VSMOW-SLAP scale, with the use of an external standard containing C_{16}–C_{30} alkanes (A-Mix, A. Schimmelmann, Indiana University, Bloomington). The dominant alkane in the majority of the samples was nC_{31}, which has been used to reflect $\delta^{2}H_{wax.}$

A known amount of internal standard (C_{46}-GDGT) was added to the GDGT fraction, after which it was filtered through a 0.45 µm PTFE filter using 99:1 (v/v) hexane:2-propanol. Samples were measured on an Agilent 1260 Infinity ultra high performance liquid chromatograph (UHPLC) coupled to an Agilent 6130 single quadrupole mass detector (MS) according to the method described by (Hopmans et al., 2016). The separation of the brGDGTs was performed on two silica Waters Acquity UPLC HEB Hilic (1.7 µm, 2.1 mm × 150 mm) columns in tandem, preceded by a guard column of the same material. The $[M + H]^+$ ions were detected in selected ion monitoring mode.

3.6. Proxy calculation

The apparent fractionation (Sauer et al., 2001), ε_{app}, reflecting net fractionation between the source water (in this case the surface waters) and soil lipids, is defined as:

$$\varepsilon_{app} = \left(\frac{\delta^2 H_{alkane} + 1000}{\delta^2 H_{water} + 1000)} - 1 \right). \quad (2)$$

All values are reported in per mille ‰ (implying a factor of 1000). Surface water δ^2H was used as a catchment integrated value of precipitation δ^2H (Hren et al., 2009; Kendall and Coplen, 2001; Bershaw et al., 2012). In the case of soil samples in the Arun that were sampled in 2011, source water was determined from the relationship between surface waters from 2012 and sample site elevation of the 2011 soil sample.

Using the fractional abundances of the brGDGTs, the MAT was determined based on the degree of methylation of 5-methyl brGDGTs (MBT′$_{5me}$; De Jonge et al., 2014b):

$$MBT'_{5me} = \frac{(Ia + Ib + Ic)}{(Ia + Ib + Ic + IIa + IIb + IIc + IIIa)}. \quad (3)$$

Temperatures derived from the GDGTs were calculated using the Bayesian regression model (BayMBT0) reported in Dearing Crampton-Flood et al. (2020), which are referred to as BayMBT MAAT hereafter. As prior input to the BayMBT0 model, the temperatures derived from the MODIS satellite (paragraph 3.6) for each individual site were used and the prior standard deviation was set at 15 following Dearing Crampton-Flood et al. (2020).

The Isomerisation ratio, (IR), was determined according to De Jonge et al. (2014b):

$$IR = \frac{IIa' + IIb' + IIc' + IIIa' + IIIb' + IIIc'}{IIa + IIb + IIc + IIIa + IIIb + IIIc + IIa' + IIb' + IIc' + IIIa' + IIIb' + IIIc'}. \quad (5)$$

3.7. Remote sensing data

MAT was derived by averaging the monthly 0.05° (approximately 5.6 km) Land Surface Temperature (LST) from 2000 to 2014 from the Moderate Resolution Imaging Spectroradiometer (MODIS) MOD11C3 product, from its first availability in 2000 until the fieldwork period (Wan and Hulley, 2015). Seasonal and annual rainfall was determined using the Tropical Rainfall Measurement Mission (TRMM) 2B31 data product averaged from 1998 to 2010, with a spatial resolution of ~5 km (Huffman et al., 2014; Bookhagen and Burbank, 2010). The seasonal and annual Enhanced Vegetation Index (EVI) was determined using MOD13C2 (MODIS) by averaging data products from 2000 to 2017 (Didan, 2015). Soil moisture in the root zone (0–100 cm) in m^3/m^3 was determined using the SMAP soil moisture SPL4SMGP data product (Reichle et al., 2016). Data were averaged from March–April–May (growing season), with a spatial resolution of 9 × 9 km. The aridity index was determined using the following equation:

$$Aridity\ \ Index = \frac{Mean\ \ Annual\ \ Precipitation}{Mean\ \ Annual\ \ Potential\ \ Evapotranspiration}, \quad (6)$$

where the mean annual precipitation derives from the aforementioned (TRMM 2B31) data product and mean annual potential evapotranspiration was determined using the Global PET dataset (Trabucco and Zomer, 2009).

4. RESULTS

4.1. Surface water and xylem water δ^2H values

In the Sutlej catchment, surface water δ^2H values ranged from −50‰ in the foreland to −112‰ in the high elevation catchments (Fig. 3A). The Alaknanda surface water δ^2H values ranged from –51 to –102‰ (Fig. 3B). The Arun surface water data ranged between –36 and–110‰ (Meese et al., 2018), which was sampled simulatneously with the soils and additional river sediments (Hoffmann et al., 2016) (Fig. 3C). The surface water δ^2H values in the Arun catchment ranged between –73 and –103‰. Surface water was sampled from both tributaries and main streams, resulting in the integration of a number of samples over a larger upstream catchment area (Table 2 Research Data). To take into account the upstream catchment sizes, surface water δ^2H values were compared using both the sample site elevation (Fig. 3) and mean catchment elevation (Fig. EA4, Electronic Annex). A negative correlation was observed between δ^2H and the mean catchment elevation in the Sutlej, Alaknanda, and Arun river catchments ($r = 0.89$, $p < 0.001$; $r = 0.91$, $p < 0.001$; and $r = 0.85$, $p < 0.01$, respectively). Moreover, a significant negative relationship was observed between surface water δ^2H and the sample site elevation in both the Sutlej and Alaknanda ($r = 0.78$, $p < 0.01$ and $r = 0.85$, $p < 0.01$, respectively) (Fig. 3A and B). The sample site elevation represents a more local δ^2H signal while the mean catchment elevation also integrates the upstream catchments of the surface waters. The isotopic lapse rates of the surface water in the Sutlej and Alaknanda catchments were 15.7 and –8.8‰ km^{-1}, respectively, when assuming a linear relationship between δ^2H and mean catchment elevation. The Arun dataset consists of surface water samples that were collected in 2011 and 2012. An extensive analysis on the factors that control the surface water δ^2H of the Arun has been previously published (Meese et al., 2018). The isotopic lapse rate of the surface waters in the Arun in 2011 and 2012 were –10.9 and –12.3‰ km^{-1}, respectively. However, since the 2011 lapse rate does not span the entire length of the transect on which the soil samples were collected, only the 2012 dataset was used in this study.

In the Khudi catchment, we did not obtain a surface water δ^2H dataset, but do have access to a daily precipitation δ^2H dataset (Fig. 3C). A significant relationship was observed between the sample site elevation and precipitation δ^2H ($r = 0.92$, $p < 0.01$). We note that this water was only sampled during the monsoon, i.e., in the same period as the soil samples were collected.

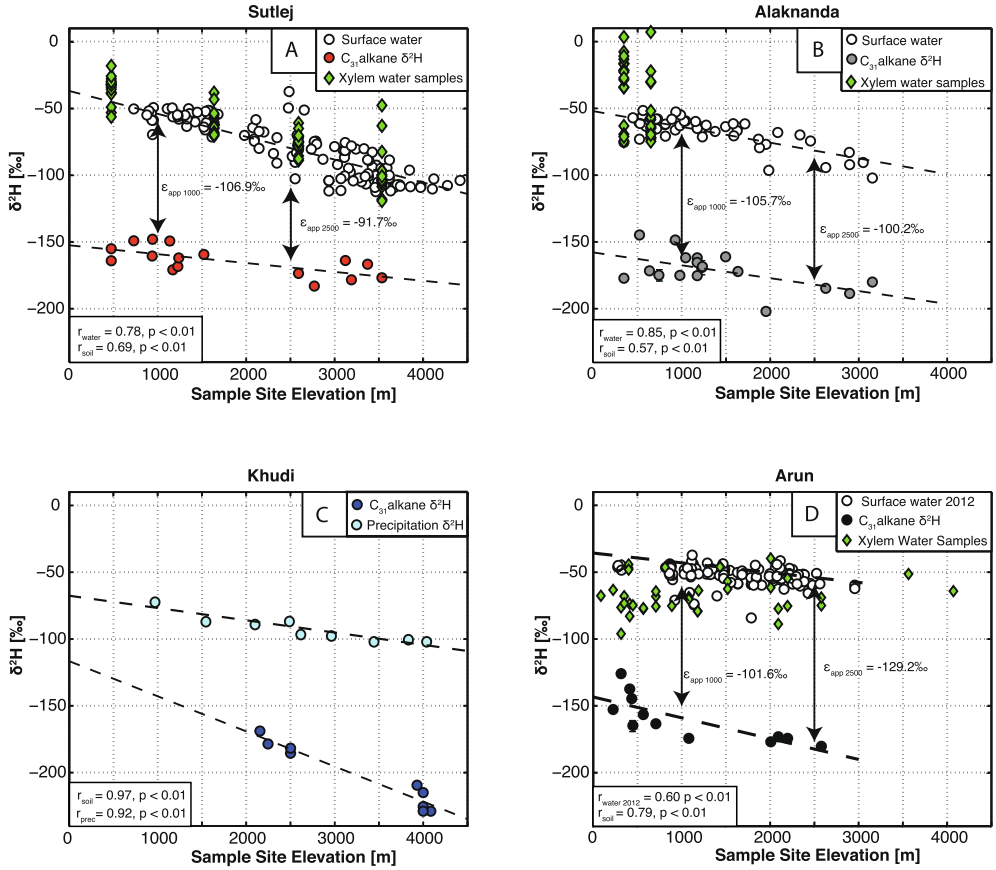

Fig. 3. Soil δ^2H of nC_{31} (red, grey, blue, and black circles) and δ^2H of tributary surface waters (white circles) and xylem waters (green diamonds) in the Sutlej, Alaknanda, Khudi and Arun catchment. ε_{app} is calculated at different elevations according to Eq. (2). The precipitation δ^2H in Fig. C is time series data from the Ghalegaon station (IAEA) http://www-naweb.iaea.org/napc/ih/IHS_resources_isohis.html. For the Arun dataset, five outliers were removed that do not represent the local precipitation signal. Thus, samples that showed a larger difference than 1500 m between sample site elevation and mean catchment elevation were removed for this reason.

Xylem water δ^2H of the Sutlej samples varied between –18.3‰ at 475 masl and –119.4‰ at 3533 masl (Fig. 3), but showed an absolute difference between the minimum and maximum of 28–82‰ between individual sample sites. The smallest range in isotope values was observed at the second highest sample site (28‰) while the largest range in isotope values was observed at the highest sample site (55‰). In the Alaknanda, xylem water ranged between 7.1‰ at 346 masl and –74.3‰ at 651 masl. High variations in the xylem water δ^2H occur along the Arun catchment, where values range between –39.7 and –96.07‰.

4.2. Soil *n*-alkane isotopic composition

The most dominant alkane in the majority of the dataset (all Sutlej and Alaknanda samples) was nC_{31}. In the following analysis, we therefore refer to the nC_{31} δ^2H values as δ^2H_{wax}. Along the Sutlej transect, δ^2H_{wax} ranged between –148 and –183‰ over an altitudinal transect from 475 to 3371 masl, the Alaknanda catchment δ^2H_{wax} ranged between –129 and –202‰ over an altitudinal transect from 346 to 3100 masl, and finally the Arun catchment values ranged between –125 and 180‰ (Fig. 3). The Khudi Khola transect is significantly shorter and steeper than the other three catchments, such that the δ^2H_{wax} ranged between –169 and –229‰, with an altitudinal transect from 1750 to 4085 masl over a distance of ~13 km, whereas the Alaknanda, Sutlej, and Arun transects are each between 160–175 km long.

We observe a significant negative correlation between δ^2H_{wax} and sample site elevation along the Sutlej, Alaknanda, Khudi, and Arun transects ($r_{Sutlej} = 0.69$, $p = 0.001$, $r_{Alaknanda} = 0.57$, $p = 0.01$, $r_{Khudi} = 0.97$, $p = 0.001$, $r_{Arun} = 0.79$, $p = 0.01$; Fig. 3). The δ^2H_{wax} with the elevation isotopic lapse rate was the lowest in the Sutlej at –6.7 (±1.8)‰ km^{-1}, –9.6 (±3.5)‰ km^{-1} for the Alaknanda, –15.6 (±3.9)‰ km^{-1} for the Arun, and –26.3 (±2.6)‰ km^{-1} in the Khudi Khola (Fig. 3).

The comparison of δ^2H of surface waters and δ^2H_{wax} in soils yielded a significant correlation in the Sutlej and Alaknanda catchment ($r = 0.56$, $p = 0.01$ and $r = 0.58$, $p = 0.01$, respectively) (Fig. 4A). In the Arun catchment, no significant correlation ($r = 0.37$, $p > 0.01$) between the δ^2H of surface waters and δ^2H of soils was observed. No values on

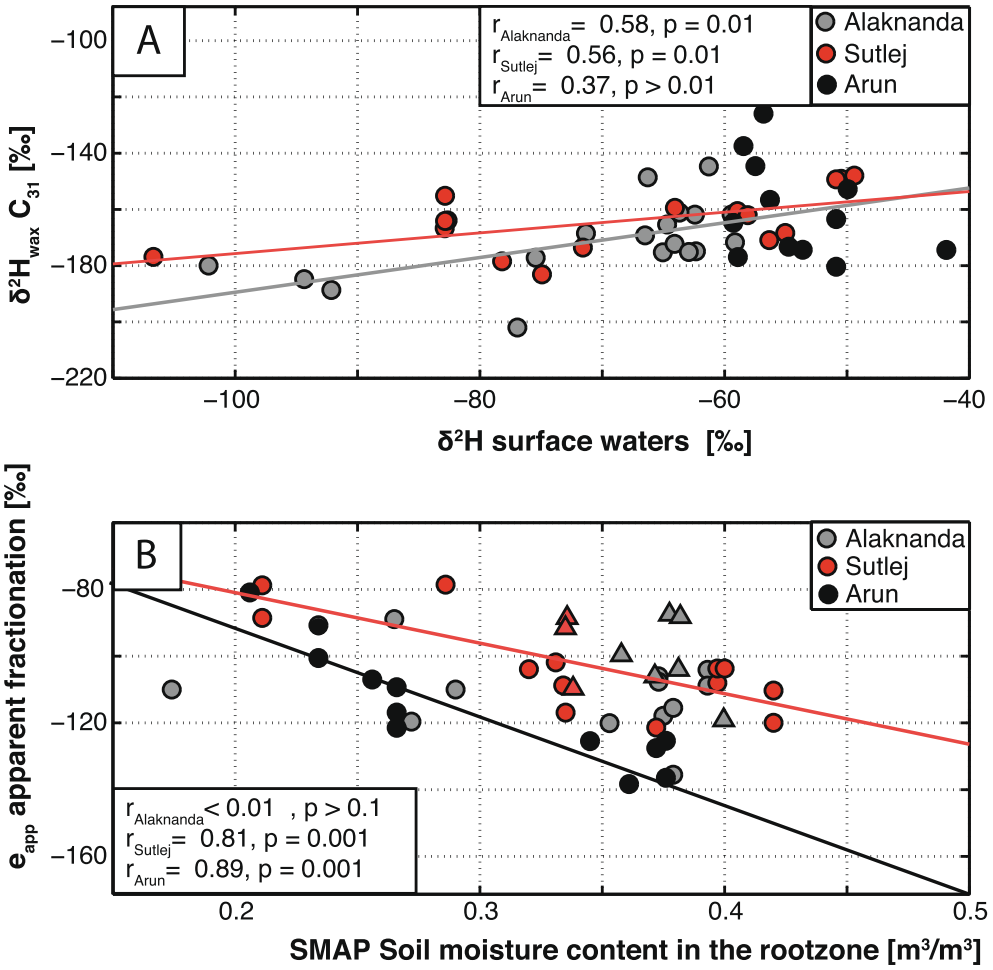

Fig. 4. A. δ^2H_{wax} nC_{31} plotted against the surface water δ^2H of the tributaries nearest the soil location. Correlation coefficients and p-values were determined with a linear regression (red and grey lines). Only regressions that are statistically significant are shown. B: Apparent fractionation versus soil moisture content in the root zone (m^3/m^3) from March–May, derived from the Soil Moisture Active Passive (SMAP) soil moisture SPL4SMGP data product (Reichle et al., 2016). Circles indicate sample sites with a predominant angiosperm vegetation cover, and triangles indicate sample sites with predominantly gymnosperms. Red and black lines are the linear regressions. Only regressions that are statistically significant are shown. (For interpretation of the references to colour in this figure legend, the reader is referred to the web version of this article.)

surface water δ^2H and ε_{app} (see below) in the Khudi are reported, as no surface water samples were collected to pair with the soils.

4.3. Apparent fractionation

Values of the apparent fractionation ε_{app} (Eq. (2)) in the Alaknanda, Sutlej, and Arun catchments have average values of –108.3, –102.1, and –112.3‰, respectively (Table 1, Research Data), but varied between –138.3 and –73.3‰ in the three transects.

A significant relationship was observed between ε_{app} and the soil moisture content in the root zone during spring (March–April–May; Reichle et al., 2016) in both the Sutlej and Arun catchment (Fig. 4B). In the Sutlej, the correlation between the soil moisture content and ε_{app} for the entire transect is significant ($r = 0.71$, $p = 0.001$). When only considering the sample sites that have predominantly *angiospermae* as vegetation cover, which are the main producers of n-alkanes (Bush and McInerney, 2013; Diefendorf et al., 2011) as opposed to gymnospermae, a higher correlation between soil moisture content and ε_{app} was observed ($r = 0.81$, $p = 0.001$). In the Alaknanda and Sutlej, where ε_{app} was relatively stable along the entire transect, no significant relationship between soil moisture in the rootzone and ε_{app} was observed (Fig. 4B).

4.4. BrGDGT thermometry

BayMBT MAAT derived from brGDGTs (Eq. (3)) varied between 3.8 °C and 23.9 °C in the Sutlej, 6.1 °C and 26.1 °C in the Alaknanda, and 5.4 °C and 20.2 °C in the Khudi Khola catchments. One of the lowest sample sites (AK6) was located on a very steep north-facing slope, receiving little to no sunlight. As a result, the BayMBT MAAT for this location was lower than expected (7.8 °C) for a sample at this elevation (523 m). We therefore identified this sample as an outlier (studentized residual

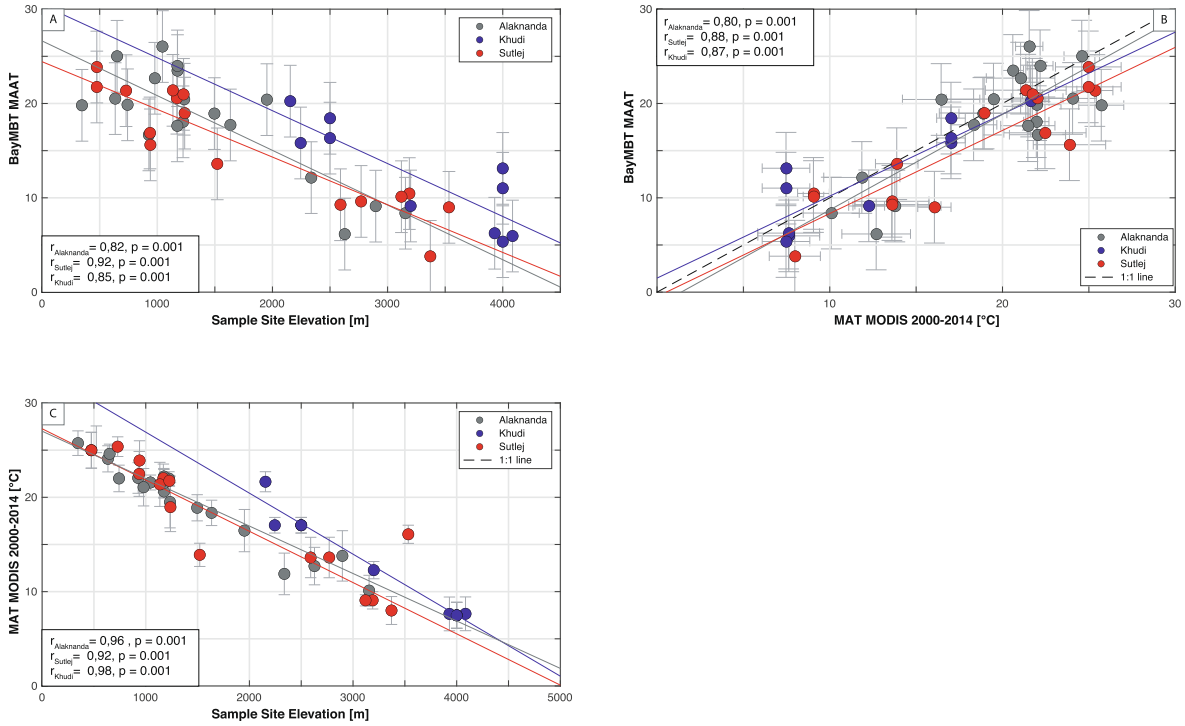

Fig. 5. BrGDGT-derived MAT for the Sutlej, Alaknanda, and Khudi catchments. A: MAT (De Jonge et al., 2014b) versus sample site elevation. B: MAT versus a 14 year average MODIS derived MAT (2000–2014, Wan and Hulley, 2015). C: MODIS MAT versus sample site elevation. Error bars represent the standard deviation from the 14-year mean MODIS temperature. Regressions were determined using a least-square weighted linear regression.

t(21) = –10.13, adjusted Bonferroni $p = 0.02$). In all transects, a significant negative correlation between BayMBT MAAT and sample site elevation was observed ($r_{Sutlej} = 0.92$, $p = 0.001$, $n = 16$, $r_{Alaknanda} = 0.82$, $p = 0.001$, $n = 19$ and $r_{Khudi} = 0.85$, $p = 0.001$, $n = 10$) (Fig. 5A). The associated temperature lapse rates in the Sutlej, Alaknanda, and Khudi were -5.1 ± 0.5 °C km^{-1}, -5.8 ± 1.1 °C km^{-1}, and -5.6 ± 1.1 °C km^{-1}, respectively (Fig. 5A).

Correlating the BayMBT MAAT with the 14-year average annual MODIS-derived MAT (from its first availability in 2000 until 2014, when our fieldwork was carried out; Wan and Hulley, 2015) for each sample location (Fig. 5B) resulted in a positive relation in all three catchments: the Sutlej catchment and the Khudi catchment both showed a highly significant correlation ($r_{Sutlej} = 0.88$, $p < 0.001$, $r_{Khudi} = 0.87$, $p < 0.001$, $r_{Alaknanda} = 0.80$) between BayMBT MAAT and MAT (MODIS).

The modern lapse rates in the three catchments were determined by correlating the 14-year MODIS derived MAT with the sample site elevation (Fig. 5C). The associated temperature lapse rates in the Sutlej, Alaknanda, and Khudi were -5.1 ± 0.6 °C km^{-1}, -5.4 ± 0.3 °C km^{-1}, and -6.5 ± 0.4 °C km^{-1}, respectively.

4.5. δ^2H and BrGDGT-derived elevation

To estimate elevation from δ^2H_{wax} data in a similar manner as in paleoelevation studies, we applied a Rayleigh distillation model to the dataset (Rowley, 2007). This exercise was performed to assess the correlation between the actual elevation of the sample site and the modeled elevation derived from the Rayleigh distillation model. This model describes the progressive isotopic depletion of a reservoir in atmospheric moisture during transport (Rowley et al., 2001) and hence depicts the ideal scenario (under ideal conditions) at the point where a moisture packet encounters an orographic barrier, which results in isotopic depletion with altitude.

The δ^2H_{wax} -based elevation reconstructions correlate significantly with the actual sample site elevation along the three transects (Alaknanda, Sutlej, and Khudi), for which both δ^2H_{wax} and brGDGTs were measured (Fig. 6A). Due to the large uncertainties associated with the Rayleigh model, the standard deviations of the elevation estimates were at a magnitude of up to 2000 m. Most samples plotted above the 1:1 line, indicating that the δ^2H_{wax} proxy generally overestimated sample site elevation. The extent of the overestimation was the largest in the lower Alaknanda (<2000 m asl), where reconstructed elevation can be up to 2500 m higher than the actual sample site elevation (Fig. 6A).

BayMBT MAAT was translated to elevation using the MODIS 14-year average temperature lapse rate of each elevation transect (Wan and Hulley, 2015). BrGDGT-based elevations were subsequently compared with the actual sample site elevation, showing a close resemblance in all three transects (Fig. 6B).

The difference in the estimated elevation from both the δ^2H_{wax} and brGDGT proxies can be visualized with the $\Delta_{Elevation}$ parameter (Fig. 6C). Soils that were sampled at

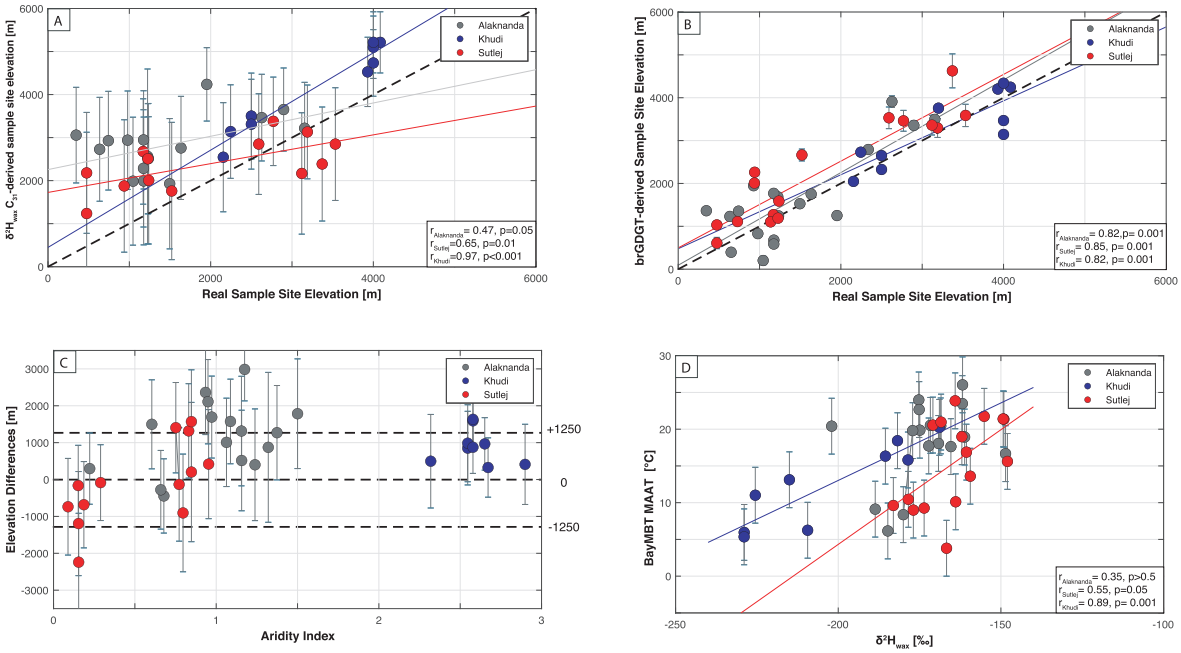

Fig. 6. A. MAT versus δ^2H_{wax}. B. BrGDGT-derived elevation versus actual sample site elevation. C. δ^2H derived elevation versus actual sample site elevation. Regressions were determined by least square weighted linear regression. D. Absolute differences between brGDGT-derived and δ^2H-derived elevation versus the Aridity index (Eq. (6)). The data points represent the difference between the actual sample site elevation and the brGDGT or δ^2H_{wax} derived sample site elevation. The standard deviations were determined by adding the brGDGT derived elevation standard deviation and δ^2H_{wax}-derived elevation standard deviations using the equation $\sigma = \sqrt{\sigma^2_{\delta 2wax} + \sigma^2_{brGDGT}}$.

arid sites (low aridity index) generally plotted under the 0-line while most of the Alaknanda and all of the Khudi samples plotted above this line.

5. DISCUSSION

5.1. Relationship between elevation and surface water δ^2H values, δ^2H_{wax}, and brGDGTs

To assess the robustness of δ^2H_{wax} and brGDGTs as a proxy for paleoelevation, the relative importance of all factors influencing these proxies other than changes in elevation must be determined. The four elevational transects along the southern Himalayan front are all characterized by different precipitation amounts, vegetation cover, and moisture sources, thus allowing us to investigate the impact of these variable parameters.

The δ^2H values of the surface waters in the Sutlej, Alaknanda, and Arun all show a significant correlation with the mean catchment elevation. Comparable lapse rates are observed in the Alaknanda and Arun surface waters (Alaknanda = –8.8‰ km^{-1}, Arun = –8.8‰ km^{-1}) (Fig. 3) while the higher lapse rate in the Sutlej (Sutlej = –15.7‰ km^{-1}) can be explained by a larger relative contribution of snow and glacial melt from tributaries in the higher elevation regions of the catchment (Wulf et al., 2016; Maurya et al., 2011; Karim and Veizer, 2002; Varay et al., 2017; Bookhagen and Burbank, 2010). The uniform direction of the lapse rates indicates that the main process controlling surface water δ^2H values is the progressive rainout of a monsoonal moisture source, i.e., the altitude effect (Gat and Confiantini, 1981). The remaining scatter in the relationship between surface water δ^2H and mean catchment elevation is possibly due to a combination of processes, such as evaporation, mixing of moisture sources with a different isotopic signature, blocking of moisture by topography, convective storms, seasonality, or contribution of snow and glacial melt, which have been observed in high elevation systems (e.g. Gat, 1996; Dansgaard, 1964; Rohrmann et al., 2014; Hughes et al., 2009; Lechler and Niemi, 2012).

The δ^2H_{wax} shows the expected negative correlation with sample site elevation in all four transects, suggesting that the first order control on the plant wax isotopic signature is precipitation δ^2H (Fig. 3). However, the different degrees of correlation between δ^2H_{wax} and the elevation in the different transects suggest that this relationship is subject to additional processes (see Section 5.2.1 for more detail).

Comparing surface water δ^2H and δ^2H_{wax} yielded a significant correlation in the Alaknanda and Sutlej, but no significant relationship in the Arun (Fig. 4A). In the Arun catchment, no significant relation was found between δ^2H_{water} and sample site elevation (Fig. 3D), which subsequently results in the absence of a relationship between δ^2H_{water} and δ^2H_{wax}. The low elevation tributaries in this area reflect the isotopic composition of ISM rainfall while the higher elevation tributaries receive elevated portions of glacial meltwater and Winter Westerly Disturbances precipitation (Meese et al., 2018). In addition, Meese et al. (2018) point out a significant difference in the isotopic composition of surface water between the sampling years (2011 and 2012). This interannual variation may have contributed

to the absence of a relation between δ^2H_{water} and δ^2H_{wax}. Scatter in the relationship between the surface water δ^2H_{water} and δ^2H_{wax} in the Sutlej and Alaknanda is most likely due to secondary processes. Surface water δ^2H reflects the isotopic signature of the upstream area, which is a mixture of precipitation, snow, and glacial melt. δ^2H_{wax} reflects a combination of source water isotopic compositions, in addition to climatic and plant physiologic drivers (Sessions et al., 1999; Chikaraishi and Naraoka, 2003; Smith and Freeman, 2006; Sachse et al., 2006, 2012; Feakins and Sessions, 2010). Our observation of an effect of moisture availability on ε_{app} (see Section 4.3) suggests that this is one factor that weakens the relationship between surface water δ^2H and δ^2Hwax.

The significant correlation between BayMBT MAAT and both sample site elevation and MODIS-derived MAT indicates that the adiabatic cooling of air mainly controls the distribution of brGDGT in the soils (Fig. 5A and B). Nevertheless, BayMBT MAAT is at times below the expected modern temperature (derived from the MODIS MAT remote sensing product) at low elevation sample sites (Fig. 5B). This offset may in part be explained by the absence of field measured temperature data, instead replaced by a 14 year average remotely sensed MODIS MAT product (Wan and Hulley, 2015). The accuracy of the MOD11C3 temperature product has been estimated to be <1 K in the range from –10 °C to +58 °C (Wan and Li, 2011), and the MODIS MAT and ground station lapse rates have been found to correlate well in previous studies in the Sutlej (Wulf et al., 2016). However, there is an ongoing discussion on what temperature data (e.g., soil or air temperature, mean annual or growing season temperature) best describes the variation in brGDGT distributions in soils (Naafs et al., 2017; Dearing Crampton-Flood et al., 2020).

5.2. Influence of water availability on soil *n*-alkane δ^2H and brGDGTs

5.2.1. Soil *n*-alkane δ^2H_{wax}

The environmental factors that influence plant δ^2H_{wax} and soil δ^2H_{wax} can be examined at two different levels. First, processes influencing a plant's moisture source (i.e., precipitation and, to a lesser degree, soil water) before it enters the plant. Second, processes that affect the isotopic composition of δ^2H_{wax} through the evaporation of leaf water from leaves (Smith and Freeman, 2006; Liu and Yang, 2008; Feakins and Sessions, 2010; Lai et al., 2006; Kahmen et al., 2013b; Sachse et al., 2012).

To characterize the offset between the source water and lipid δ^2H, the apparent fractionation (ε_{app}) was calculated (Eq. (2)). The apparent fractionation incorporates the influence of evapotranspiration, soil evaporation, and plant physiology, and is directly linked to the variation in the relative humidity and precipitation in the study area (Smith and Freeman, 2006; Sachse et al., 2006). However, the ε_{app} in this study is used to describe the offset between the surface water δ^2H and δ^2H_{wax}. Surface water δ^2H is assumed to be an annual integrated precipitation δ^2H signal, but glacier/snowmelt, seasonality in precipitation, and evaporation may influence the isotopic signature of surface water δ^2H. Moreover, the apparent fractionation integrates both evaporative effects and biosynthetic fractionation, complicating attempts to decipher the degree of impact from both factors individually (Sachse et al., 2006; Smith and Freeman, 2006; Feakins and Sessions, 2010; Kahmen et al., 2013a; Sessions et al., 1999).

In the Sutlej, Alaknanda, and Arun catchments, the apparent fractionation changes with elevation (Fig. 3A, B, and D). Unfortunately, along the Khudi elevation transect, no surface water samples coupled to the soil sampling locations were taken (Fig. 3C), preventing us from testing this relationship in this catchment. Values of apparent fractionation in the Sutlej, Alaknanda, and Arun are similar to the ε_{app} between soil alkane δ^2H and surface waters observed in other elevation transects on the SE Tibetan Plateau (Bai et al., 2015), but lower than other surface soil studies located on the Tibetan Plateau (Luo et al., 2011; Jia et al., 2008; Wang et al., 2017).

Soil evaporation enriches δ^2H in soil water and causes a decrease in the ε_{app} in arid regions (Smith and Freeman, 2006; Polissar and Freeman, 2010). A decrease in the apparent fractionation with increasing elevation is observed along the Sutlej and Alaknanda transect, which are the two transects that receive the lowest amount of precipitation at high elevation sample sites (Figs. 2 and 3). This decrease in ε_{app} with increasing elevation suggests that aridity has an effect on the soil δ^2H_{wax} values in the high elevation Sutlej and Alaknanda samples. The same pattern is observed when using xylem water δ^2H to calculate the ε_{app}; however, we regard surface water δ^2H values as better integrators (both spatial and temporal) compared to single plant xylem water values, which is supported by the observed scatter in the xylem water δ^2H values (Fig. 3).

In addition, in the Arun transect, a significant negative correlation was observed between ε_{app} and the Soil Moisture Content (Fig. 4B) (SMC; Reichle et al., 2016). A decrease in the apparent fractionation under drier conditions reflects increasing leaf and/or soil water evaporative ^2H-enrichment, which has been observed in previous studies (Kahmen et al., 2013b; Polissar and Freeman, 2010; Schwab et al., 2015). Moreover, a higher correlation was observed between ε_{app} and SMC in the rootzone when only considering the soil sample sites with *angiospermae* in the Sutlej transect (Fig. 4B, circles). *Gymnospermae* modify their leaf waxes in a different manner (having higher photosynthetic discrimination) when subject to specific environmental stress, and display lower stomatal conductance for CO_2 and H_2O vapor in comparison with *angiospermae*, resulting in a different relationship between surface water δ^2H and δ^2H_{wax} (Tipple et al., 2013; Pedentchouk et al., 2008; Diefendorf et al., 2011).

However, in the Alaknanda transect, no significant correlation between ε_{app} and any of the previously mentioned hydrological parameters was observed. This suggests that aridity is not the main controlling factor that determines ε_{app}, or that the surface water δ^2H values were not representative of the local conditions at the soil sampling sites in the Alaknanda. We relate the apparent fractionation to the soil moisture content to show that, in drier areas (low soil

moisture content), the apparent fractionation is smaller. Therefore, we show that assuming a constant apparent fractionation, as is often done, is strictly not valid. Moreover, changes in climatic conditions during mountain range uplift, such as rainshadow development, should be taken into account when interpreting paleoelevation/paleoclimate records in such settings, as been introduced by Rohrmann et al. (2016)

5.2.2. BrGDGTs

In a similar manner as with the lipid δ^2H_{wax} proxy, confounding factors that may alter the brGDGT distribution in soils also influence the brGDGT temperature proxy. The most important factors that were found to have an impact on the relationship between brGDGTs and temperature are soil pH and moisture availability (Weijers et al., 2007). These influences become especially important in arid regions (MAP < 500 mm), where moisture availability appears to explain a larger part of the variation in the brGDGT distribution than temperature (Dirghangi et al., 2013; Wang et al., 2014; Menges et al., 2014; Peterse et al., 2012; Dang et al., 2016). Based on brGDGT distributions in a soil transect with a large range in moisture content (0–61%), Dang et al. (2016) suggested that 6-methyl brGDGTs especially respond to variations in the moisture content rather than to MAT. Consequently, they proposed that only sites where the contribution of 6-methyl brGDGTs is low, defined by an isomerisation ratio (IR; Eq. (5)) < 0.5, can be used to reliably reconstruct MAT (Dang et al., 2016; Naafs et al., 2017). Interestingly, for most sites (>75%) in the Alaknanda and Sutlej catchments the IR is significantly above 0.5, whereas the relationship between BayMBT MAAT and elevation, as well as between BayMBT MAAT and MODIS MAT, is good (Fig. 5). Moreover, there is no trend between SMC and the relative distribution of brGDGTs, suggesting that moisture content does not influence brGDGT distributions in Himalaya transects, and, more importantly, that the use of IR is generally not a valid method for discarding samples for (paleo-) temperature reconstruction (Table 4, Research Data).

5.3. Combination of brGDGTs and *n*-alkane δ^2H as a more robust elevation proxy

The dual application of brGDGTs and δ^2H_{wax} has been used to assess the effect that varying environmental conditions have on their potential as elevation proxies (Ernst et al., 2013; Nieto-Moreno et al., 2016; Wang et al., 2017; Hren et al., 2010; Peterse et al., 2009). Although these studies analyzed both proxies in the same set of samples, their performance has thus far only been assessed separately. Here, we test the potential of the actual combination of brGDGTs and δ^2H in an elevation context, with the aim to improve their use as a reliable paleoelevation proxy.

Both the δ^2H_{wax} and brGDGT proxy are used to reconstruct elevation, but the individual proxies record different processes that indirectly cause their changes with increasing elevation (i.e., Rayleigh distillation and adiabatic cooling of air). The strongest correlation between these proxies is found along the Khudi transect, suggesting that both proxies are suitable for elevation reconstruction in this catchment (Fig. 6A). The Khudi transect is relatively short and does not encompass large changes in hydrology (i.e., it is generally wet, with a mean annual precipitation above 3000 mm/year), as well as that environmental conditions vary less here than in the other transects. The Sutlej shows a significant correlation between δ^2H_{wax} and reconstructed MAT ($r = 0.55$, $p = 0.05$), but with a substantial amount of scatter, while in the Alaknanda no significant correlation ($r = 0.35$, $p > 0.5$) was observed (Fig. 6D). The previously mentioned climatic conditions and geomorphological/phy siological processes influencing either the δ^2H_{wax} or BayMBT MAAT may be the cause of this scatter.

In an attempt to combine these two proxies and observe to what extent this can improve elevation reconstruction reliability, we assessed the differences in estimated elevation between the proxies (Fig. 6C), where the difference is indicated as $\Delta_{Elevation}$:

$$\Delta_{Elevation} = \delta^2H_{Elevation} - brGDGT_{Elevation} \quad (7)$$

To assess the influence of changing hydrological conditions, $\Delta_{Elevation}$ is compared to the aridity index (Eq. (6)) of each sample location. The majority of the sites plot within a 1250 m range from the 0-line, indicating that both proxies yield comparable elevation estimates that are less than 1250 m offset (Fig. 6C), which is within the same range of error reported in studies that use these proxies to reconstruct paleo-elevation, e.g., the Sierra Nevada and Tibetan Plateau (Hren et al., 2010; Zhuang et al., 2014). In the trans-Himalayan transects of this study, the good relation between brGDGT-derived elevation and the actual elevation indicates that brGDGTs can be considered a good predictor of elevation (Fig. 6B). Nevertheless, brGDGTs increasingly overestimate sample site elevation towards the lowlands, likely as an artifact of proxy saturation, as MBT'_{5me} values near 1 at these sites (Table 4, Research Data). Hence, the MBT'_{5me} value can be used as an indicator of the accuracy of the reconstructed elevation for each site. On the other hand, δ^2H_{wax} is associated with large errors, primarily subject to influences from aridity and soil moisture availability.

In general, samples with negative $\Delta_{Elevation}$ values are located in areas that are either experiencing arid conditions, or located behind an orographic barrier, resulting in moisture blocking (Galewsky, 2009; Hughes et al., 2009). Samples with a positive $\Delta_{Elevation}$ offset may be located in areas with high moisture, where the relationships between δ^2H_{wax} and elevation can become distorted by the amount effect, as shown in Peterse et al. (2009). This suggests that, in a multiproxy study, the use of both δ^2H_{wax} and brGDGTs can provide information on the hydrological conditions of the (paleo-) soils using the $\Delta_{Elevation}$ parameter. For example, the formation of soils during arid conditions can result in large offsets between the reconstructed elevation and actual sample site elevation. We therefore suggest that soils that show a large negative offset ($\Delta_{Elevation}$ value outside of the 1250 m error bars) between the δ^2H_{wax} and brGDGT proxies should be interpreted with caution, as these samples can be influenced by arid conditions during formation.

6. CONCLUSIONS

Both leaf wax *n*-alkane δ^2H values and brGDGTs primarily record a climatic parameter that changes with elevation, although additional processes influence these compositions. We found that the δ^2H_{wax} values in the Sutlej, Alaknanda, and Arun generally record surface water δ^2H values. Scatter in this relationship is attributed to the possibility that surface water δ^2H values did not represent the local conditions at the soil sampling sites, as well as the influence of aridity on the δ^2H_{wax} signature stored in soils. We confirm this via an observed dependency of the apparent fractionation between the soil δ^2H_{wax} and surface water δ^2H in the Sutlej catchment with soil moisture availability, as well as based on the vegetation type.

The BayMBT MAAT in the same three transects showed a high correlation with both sample site elevations and MODIS-derived MAT. To improve the accuracy of paleo-elevation studies, a combined approach between the δ^2H and brGDGT proxy could be applied. Large offsets (above 1250 m) between elevations inferred from both proxies ($\Delta_{Elevation}$) should be interpreted with caution, and could be affected by moisture availability/aridity, the amount effect in precipitation, or originate from locations with high annual temperatures. In the case of a large offset, where MBT'_{5me} values are <1, the proposed $\Delta_{Elevation}$ parameter can provide information on the hydrological setting of the depositional environment of these soils.

In conclusion, the results of this study show that both the δ^2H_{wax} and brGDGT proxies are optimal in a relatively stable climate (as the shorter Khudi transect suggests), but are significantly influenced by variable hydrology, i.e., increasing aridity (as is often the case in orogenic settings with high altitude plateaus). Our results contribute to the existing literature on organic proxies, showing that the application of a combined proxy approach could provide information on the hydrological characteristics of the depositional environment. The uncertainties in elevation estimates due to moisture availability and high temperatures emphasize that prior knowledge of the tectonic setting is crucial when reconstructing elevations.

Declaration of Competing Interest

The authors declare that they have no known competing financial interests or personal relationships that could have appeared to influence the work reported in this paper.

ACKNOWLEDGEMENTS

A Marie Curie ITN (iTECC) funded Iris van der Veen and Jesse Davenport, Dirk Sachse was funded by a DFG Emmy Noether (SA1889/1-1) grant and the ERC Consolidator grant STEEPclim (grant no. 647035). NWO grant no. 834.11.006 enabled the purchase of the UHPLC–MS system used for GDGT analyses at the UU. Francien Peterse acknowledges financial support from NWO-Veni grant no. 863.13.0016. We thank Viktor Evrard and Thomas Rigaudier for technical lab support, Guillaume Morin for sampling soils in Nepal, and Tashi Jigmet for field assistance. We thank the editors for their time and valuable remarks and the three anonymous reviewers for their constructive comments.

RESEARCH DATA

Research data associated with this manuscript can be accessed through DOI: 10.17632/cvdnf723k5.1.

APPENDIX A. SUPPLEMENTARY MATERIAL

Supplementary data to this article can be found online at https://doi.org/10.1016/j.gca.2020.09.014.

REFERENCES

Bai Y., Fang X., Jia G., Sun J., Wen R. and Ye Y. (2015) Different altitude effect of leaf wax n-alkane δD values in surface soils along two vapor transport pathways, southeastern Tibetan Plateau. *Geochim. Cosmochim. Acta* **170**, 94–107.

Bershaw J., Penny S. M. and Garzione C. N. (2012) Stable isotopes of modern water across the Himalaya and eastern Tibetan Plateau: Implications for estimates of paleoelevation and paleoclimate. *J. Geophys. Res.: Atmos.* **117**, 1–18.

Bookhagen B. and Burbank D. W. (2006) Topography, relief, and TRMM-derived rainfall variations along the Himalaya. *Geophys. Res. Lett.* **33**, L08405.

Bookhagen B. and Burbank D. W. (2010) Toward a complete Himalayan hydrological budget: Spatiotemporal distribution of snowmelt and rainfall and their impact on river discharge. *J. Geophys. Res. Earth Surf.* **115**, F03019.

Bookhagen B., Thiede R. C. and Strecker M. R. (2005) Abnormal monsoon years and their control on erosion and sediment flux in the high, arid northwest Himalaya. *Earth Planet. Sci. Lett.* **231**, 131–146.

Bush R. T. and McInerney F. A. (2013) Leaf wax n-alkane distributions in and across modern plants: Implications for paleoecology and chemotaxonomy. *Geochim. Cosmochim. Acta* **117**, 161–179.

Cannon F., Carvalho L. M. V., Jones C. and Bookhagen B. (2014) Multi-annual variations in winter westerly disturbance activity affecting the Himalaya. *Clim. Dyn.* **44**, 441–455.

Chikaraishi Y. and Naraoka H. (2003) Compound-specific δD-δ13C analyses of n-alkanes extracted from terrestrial and aquatic plants. *Phytochemistry* **63**, 361–371.

Clift P. D., Hodges K. V., Heslop D., Hannigan R., van Long H. and Calves G. (2008) Correlation of Himalayan exhumation rates and Asian monsoon intensity. *Nat. Geosci.* **1**, 875–880.

Coffinet S., Huguet A., Williamson D., Fosse C. and Derenne S. (2014) Potential of GDGTs as a temperature proxy along an altitudinal transect at Mount Rungwe (Tanzania). *Org. Geochem.* **68**, 82–89.

Coffinet S., Huguet A., Pedentchouk N., Bergonzini L., Omuombo C., Williamson D., Anquetil C., Jones M., Majule A., Wagner T. and Derenne S. (2017) Evaluation of branched GDGTs and leaf wax n-alkane δ2H as (paleo) environmental proxies in East Africa. *Geochim. Cosmochim. Acta* **198**, 182–193.

Dang X., Yang H., Naafs B. D. A., Pancost R. D. and Xie S. (2016) Evidence of moisture control on the methylation of branched glycerol dialkyl glycerol tetraethers in semi-arid and arid soils. *Geochim. Cosmochim. Acta* **189**, 24–36.

Dansgaard W. (1964) Stable isotopes in precipitation. *Tellus* **16**, 436–468.

Dash S. K., Kulkarni M., Mohanty U. C. and Prasad K. (2009) Changes in the characteristics of rain events in India. *J. Geophys. Res.* **114**, D10109.

Davtian N., Ménot G., Bard E., Poulenard J. and Podwojewski P. (2016) Consideration of soil types for the calibration of molecular proxies for soil pH and temperature using global soil datasets and Vietnamese soil profiles. *Org. Geochem.* **101**, 140–153.

Dearing Crampton-Flood E., Tierney J. E., Peterse F., Kirkels F. M. S. A. and Sinninghe Damsté K. S. (2020) BayMBT: A Bayesian calibration model for branched glycerol dialkyl glycerol tetraethers in soils and peats. *Geochim. Cosmochim. Acta* **268**, 142–159.

Dettman D. L., Fang X., Garzione C. N. and Li J. (2003) Uplift-driven climate change at 12 Ma: A long δ18O record from the NE margin of the Tibetan plateau. *Earth Planet. Sci. Lett.* **214**, 267–277.

De Jonge C., Stadnitskaia A., Hopmans E. C., Cherkashov G., Fedotov A. and Sinninghe Damsté J. S. (2014a) In situ produced branched glycerol dialkyl glycerol tetraethers in suspended particulate matter from the Yenisei River, Eastern Siberia. *Geochim. Cosmochim. Acta* **125**, 476–491.

De Jonge C., Hopmans E. C., Zell C. I., Kim J. H., Schouten S. and Sinninghe Damsté J. S. (2014b) Occurrence and abundance of 6-methyl branched glycerol dialkyl glycerol tetraethers in soils: Implications for palaeoclimate reconstruction. *Geochim. Cosmochim. Acta* **141**, 97–112.

De Jonge C., Radujković D., Sigurdsson B. D., Weedon J. T., Janssens I. and Peterse F. (2019) Lipid biomarker temperature proxy responds to abrupt shift in the bacterial community composition in geothermally heated soils. *Org. Geochem.* **137**, 103897.

Didan, K., 2015. MOD13C2 MODIS/Terra Vegetation Indices Monthly L3 Global 0.05Deg CMG V006. NASA EOSDIS Land Processes DAAC.

Diefendorf A. F., Freeman K. H., Wing S. L. and Graham H. V. (2011) Production of n-alkyl lipids in living plants and implications for the geologic past. *Geochim. Cosmochim. Acta* **75**, 7472–7485.

Dirghangi S. S., Pagani M., Hren M. T. and Tipple B. J. (2013) Distribution of glycerol dialkyl glycerol tetraethers in soils from two environmental transects in the USA. *Org. Geochem.* **59**, 49–60.

Ernst N., Peterse F., Breitenbach S. F. M., Syiemlieh H. J. and Eglinton T. (2013) Biomarkers record environmental changes along an altitudinal transect in the wettest place on Earth. *Org. Geochem.* **60**, 93–99.

Feakins S. J. and Sessions A. L. (2010) Controls on the D/H ratios of plant leaf waxes in an arid ecosystem. *Geochim. Cosmochim. Acta* **74**, 2128–2141.

Galewsky J. (2009) Orographic precipitation isotopic ratios in stratified atmospheric flows: Implications for paleoelevation studies. *Geology* **37**, 791–794.

Garzione C. N., Dettman D. L., Quade J., DeCelles P. G. and Butler R. F. (2000a) High times on the Tibetan Plateau: Paleoelevation of the Thakkhola graben, Nepal. *Geology* **28**, 339–342.

Garzione C. N., Quade J., DeCelles P. G. and English N. B. (2000b) Predicting paleoelevation of Tibet and the Himalaya from δ18O vs. altitude gradients in meteoric water across the Nepal Himalaya. *Earth Planet. Sci. Lett.* **183**, 215–229.

Gat J. R. (1996) Oxygen and Hydrogen Isotopes in the Hydrologic Cycle. *Annu. Rev. Earth Planet. Sci.* **24**, 225–262.

Gat J. R. and Confiantini R. (1981) Stable isotope hydrology: Deuterium and oxygen-18 in the water cycle. *IAEA Tech. Rep. Ser.* **210**, 339.

Gat J. R., Mook W. G. and Meyer H. AJ. (2000) Observed isotope effects in precipitation. *Vol. II: Atmos. Water* **2**, 43–62.

Hoffmann B., Feakins S. J., Bookhagen B., Olen S. M., Adhikari D. P., Mainali J. and Sachse D. (2016) Climatic and geomorphic drivers of plant organic matter transport in the Arun River, E Nepal. *Earth Planet. Sci. Lett.* **452**, 104–114.

Hopmans E., Schouten S. and Sinninghe Damsté J. S. (2016) The effect of improved chromatography chromatography on GDGT-based palaeoproxies. *Org. Geochem.* **93**, 1–6.

Hou J., D'Andrea W. J. and Huang Y. (2008) Can sedimentary leaf waxes record D/H ratios of continental precipitation? Field, model, and experimental assessments. *Geochim. Cosmochim. Acta* **72**, 503–3517.

Hren M. T., Bookhagen B., Blisniuk P. M., Booth A. L. and Chamberlain C. P. (2009) $\delta^{18}O$ and δD of streamwaters across the Himalaya and Tibetan Plateau: Implications for moisture sources and paleoelevation reconstructions. *Earth Planet. Sci. Lett.* **288**, 20–32.

Hren M. T., Pagani M., Erwin D. M. and Brandon M. (2010) Biomarker reconstruction of the early Eocene paleotopography and paleoclimate of the northern Sierra Nevada. *Geology* **38**, 7–10.

Huang Y., Human B., Wang Y. and Webb, III, T. (2004) Hydrogen isotope ratios of individual lipids in lake sediments as novel tracers of climatic and environmental change: a surface sediment test. *J. Paleolimnol.* **31**, 363–375.

Huffman, G.J., Stocker, D.T., Bolvin, E.J., Nelkin, 2014. TRMM3B42 3-Hour Realtime TRMM Multi-satellite Precipitation Analysis. NASA/GSFC, Greenbelt, MD, USA, ftp://arthurhou.pps.eosdis.nasa.gov/trmmdata/.

Hughes M., Hall A. and Fovell R. G. (2009) Blocking in areas of complex topography, and its influence on rainfall distribution. *J. Atmos. Sci.* **66**, 508–518.

Jaeschke A., Rethemeyer J., Lappé M., Schouten S., Boeckx P. and Schefuß E. (2018) Influence of land use on distribution of soil n-alkane ΔD and BrGDGTs along an altitudinal transect in Ethiopia: Implications for (Paleo)environmental studies. *Org. Geochem.* **124**, 77–87.

Jia G., Wei K., Chen F. and Peng P. (2008) Soil n-alkane δD vs. altitude gradients along Mount Gongga, China. *Geochim. Cosmochim. Acta* **72**, 5165–5174.

Kahmen A., Schefuß E. and Sachse D. (2013a) Leaf water deuterium enrichment shapes leaf wax n-alkane δD values of angiosperm plants I: Experimental evidence and mechanistic insights. *Geochim. Cosmochim. Acta* **111**, 39–49.

Kahmen A., Hoffmann B., Schefuß E., Arndt S. K., Cernusak L. A., West J. B. and Sachse D. (2013b) Leaf water deuterium enrichment shapes leaf wax n-alkane δD values of angiosperm plants II: Observational evidence and global implications. *Geochim. Cosmochim. Acta* **111**, 50–63.

Karim A. and Veizer J. (2002) Water balance of the Indus River Basin and moisture source in the Karakoram and western Himalayas: Implications from hydrogen and oxygen isotopes in river water. *J. Geophys. Res.: Atmos.* **107**, 1–12.

Kendall C. and Coplen T. B. (2001) Distribution of oxygen-18 and deuteriun in river waters across the United States. *Hydrol. Process.* **15**, 363–1393.

Lai C.-T., Ehleringer J. R., Bond B. J. and Paw K. T. (2006) Contributions of evaporation, isotopic non-steady state transpiration and atmospheric mixing on the delta18O of water vapour in Pacific Northwest coniferous forests. *Plant Cell Environ.* **29**, 77–94.

Lechler A. R. and Niemi N. A. (2012) The influence of snow sublimation on the isotopic composition of spring and surface waters in the southwestern United States: Implications for stable isotope – based paleoaltimetry and hydrologic studies. *GSA Bull.* **3**, 18–334.

Liu W. and Yang H. (2008) Multiple controls for the variability of hydrogen isotopic compositions in higher plant n-alkanes from modern ecosystems. *Glob. Change Biol.* **14**, 2166–2177.

Luo P., Peng P., Gleixner G., Zheng Z., Pang Z. and Ding Z. (2011) Empirical relationship between leaf wax n-alkane δD and altitude in the Wuyi, Shennongjia and Tianshan Mountains, China: Implications for paleoaltimetry. *Earth Planet. Sci. Lett.* **301**, 285–296.

Maurya A. S., Shah M., Deshpande R. D., Bhardwal R. M., Prasad A. and Gupta S. K. (2011) Hydrograph separation and precipitation source identification using stable water isotopes and conductivity: River Ganga at Himalayan foothills. *Hydrol. Process.* **25**, 1521–1530.

Meese B., Bookhagen B., Olen S. M., Barthold F. and Sachse D. (2018) The effect of Indian Summer Monsoon rainfall on surface water δD values in the central Himalaya. *Hydrol. Process.* **32**, 3662–3674.

Menges J., Huguet C., Alcañiz J. M., Fietz S., Sachse D. and Rosell-Melé A. (2014) Influence of water availability in the distributions of branched glycerol dialkyl glycerol tetraether in soils of the Iberian Peninsula. *Biogeosciences* **11**, 2571–2581.

Molnar P. and England P. (1990) Late Cenozoic uplift of mountain ranges and global climate change: chicken or egg? *Nature* **346**, 29–34.

Naafs B. D. A., Gallego-Sala A. V., Inglis G. N. and Pancost R. D. (2017) Refining the global branched glycerol dialkyl glycerol tetraether (brGDGT) soil temperature calibration. *Org. Geochem.* **106**, 48–56.

Newberry S. L., Nelson D. B. and Kahmen A. (2017) Cryogenic vacuum artifacts do not affect plant water-uptake studies using stable isotope analysis. *Ecohydrology* **10**, 1892.

Nieto-Moreno V., Rohrmann A., van der Meer M. T. J., Sinninghe Damsté J. S., Sachse D., Tofelde S., Niedermeyer E. M., Strecker M. R. and Mulch A. (2016) Elevation-dependent changes in n-alkane δD and soil GDGTs across the South Central Andes. *Earth Planet. Sci. Lett.* **453**, 234–242.

Pedentchouk N., Sumner W., Tipple B. and Pagaini M. (2008) $\delta^{13}C$ and δD compositions of n-alkanes from modern angiosperms and conifers: An experimental set up in central Washington State, USA. *Org. Geochem.* **39**, 1066–1071.

Peterse F., van der Meer M. T. J., Schouten S., Jia G., Ossebaar J., Blokker J. and Sinninghe Damsté J. S. (2009) Assessment of soil n-alkane δD and branched tetraether membrane lipid distributions as tools for paleoelevation reconstruction. *Biogeosci. Discuss.* **6**, 2799–2807.

Peterse F., van der Meer M. T. J., Schouten S., Weijers J. H. W., Fierer N., Jackson R. B., Kim J.-H. and Sinninghe Damsté J. S. (2012) Revised calibration of the MBT-CBT paleotemperature proxy based on branched tetraether membrane lipids in surface soils. *Geochim. Cosmochim. Acta* **96**, 215–229.

Polissar P. J., Freeman K. H., Rowley D. B., McInerney F. A. and Currie B. S. (2009) Paleoaltimetry of the Tibetan Plateau from D/H ratios of lipid biomarkers. *Earth Planet. Sci. Lett.* **287**, 64–76.

Polissar P. J. and Freeman K. H. (2010) Effects of aridity and vegetation on plant-wax δD in modern lake sediments. *Geochim. Cosmochim. Acta* **74**, 5785–5797.

Poulsen C. J., Ehlers T. A. and Insel N. (2010) Onset of convective rainfall during gradual late miocene rise of the Central Andes. *Science* **328**, 490–493.

Quade J., Garzione C. N. and Eiler J. M. (2007) Paleoelevation reconstruction using pedogenic carbonates. *Rev. Mineral. Geochem.* **66**, 53–87.

Reichle, R., De Lannoy, G., Koster, R.D., Crow, W.T., Kimball, J. S., 2016. SMAP L4 9 km EASE-Grid Surface and Root Zone Soil Moisture Geophysical Data, Version 2. [SPL4SMAU]. NASA National Snow and Ice Data Center Distributed Active Archive Center, Boulder, Colorado, USA.

Rohrmann A., Sachse D., Mulch A., Pingel H., Tofelde S., Alonso R. and Strecker M. (2016) Miocene orographic uplift forces rapid hydrological change in the southern central Andes. *Sci. Rep.* **6**, 35678.

Rohrmann A., Strecker M. R., Bookhagen B., Mulch A., Sachse D., Pingel H., Alonso R. N., Schildgen T. F. and Montero C. (2014) Can stable isotopes ride out the storms? The role of convection for water isotopes in models, records, and paleoaltimetry studies in the central Andes. *Earth Planet. Sci. Lett.* **407**, 187–195.

Rowley D. B. (2007) Stable isotope-based paleoaltimetry: Theory and validation. *Rev. Mineral. Geochem.* **66**, 23–52.

Rowley D. B., Pierrehumbert R. T. and Currie B. S. (2001) A new approach to stable isotope-based paleoaltimetry: Implications for paleoaltimetry and paleohypsometry of the High Himalaya since the late Miocene. *Earth Planet. Sci. Lett.* **188**, 253–268.

Sachse D., Billault I., Bowen G. J., Chikaraishi Y., Dawson T. E., Feakins S. J., Freeman K. H., Magill C. R., McInerney F. A., van der Meer M. T. J., Polissar P., Robins R. J., Sachs J. P., Schmidt H. J., Sessions A. L., White J. W. C., West J. B. and Kahmen A. (2012) Molecular paleohydrology: Interpreting the hydrogen-isotopic composition of lipid biomarkers from photosynthesizing organisms. *Annu. Rev. Earth Planet. Sci.* **40**, 221–249.

Sachse D., Radke J. and Gleixner G. (2004) Hydrogen isotope ratios of recent lacustrine sedimentary n-alkanes record modern climate variability. *Geochim. Cosmochim. Acta* **68**, 4877–4889.

Sachse D., Radke J. and Gleixner G. (2006) δD values of individual n-alkanes from terrestrial plants along a climatic gradient – Implications for the sedimentary biomarker record. *Org. Geochem.* **37**, 469–483.

Sauer P. E., Eglinton T. I., Hayes J. M., Schimmelman A. and Sessions A. L. (2001) Compound-specific D/H ratios of lipid biomarkers from sediments as a proxy for environmental and climatic conditions. *Geochim. Cosmochim. Acta* **65**, 213–222.

Schwab V. F., Garcin Y., Sachse D., Todou G., Séné O., Onana J.-M., Achoundong G. and Gleixner G. (2015) Effect of aridity on $\delta^{13}C$ and δD values of C3 plant- and C4 graminoid-derived leaf wax lipids from soils along an environmental gradient in Cameroon (Western Central Africa). *Org. Geochem.* **78**, 99–109.

Sessions A. L., Burgoyne T. W., Schimmelman A. and Hayes J. M. (1999) Fractionation of hydrogen isotopes in lipid biosynthesis. *Org. Geochem.* **30**, 1193–1200.

Singh J. S. and Singh S. P. (1987) Forest vegetation of the Himalaya. *Bot. Rev.* **53**, 80–192.

Sinninghe Damsté J. S., Ossebaar J., Schoutjern S. and Verschuren D. (2008) Altitudinal shifts in the branched tetraether lipid distribution in soil from Mt. Kilimanjaro (Tanzania): Implications for the MBT/CBT continental palaeothermometer. *Org. Geochem.* **39**, 1072–1076.

Smith F. A. and Freeman K. H. (2006) Influence of physiology and climate on δD of leaf wax n-alkanes from C3 and C4 grasses. *Geochim. Cosmochim. Acta* **70**, 1172–1187.

Tipple B. J., Berke M. A., Doman C. E., Khachaturyan S. and Ehleringer J. R. (2013) Leaf-wax n-alkanes record the plant-water environment at leaf flush. *PNAS* **110**, 2659–2664.

Trabucco, A., Zomer, R.J., 2009. Global Aridity Index (Global-Aridity) and Global Potential Evapo-Transpiration (Global-PET) Geospatial Database, CGIAR Consortium for Spatial Information. www.Cgiar-Csi.Org.

USGS, 2006. Shuttle Radar Topography Mission, 3Arc Second Scene. Global Land Cover Facility. University of Maryland, College Park, MD.

Varay L. S., Rai S. P., Singh S. K. and Jain V. (2017) Estimation of snow and glacial melt contribution through stable isotopes and assessment of its impact on river morphology through stream power approach in two Himalayan river basins. *Environ. Earth Sci.* **76**, 809.

Wan, Z., Hulley, G., 2015. MOD11C3 MODIS/Terra Land Surface Temperature/Emissivity Monthly L3 Global 0.05Deg CMG V006. NASA EOSDIS Land Processes DAAC.

Wan Z. and Li Z.-L. (2011) MODIS land surface temperature and emissivity. *Land Remote Sensing and Global Environmental Change* **894**.

Wang C., Hren M. T., Hoke G. D., Liu-Zeng J. and Garzione C. N. (2017) Soil n-alkane δD and glycerol dialkyl glycerol tetraether (GDGT) distributions along an altitudinal transect from southwest China: Evaluating organic molecular proxies for paleoclimate and paleoelevation. *Org. Geochem.* **107**, 21–32.

Wang H., Liu W. and Zhang C. L. (2014) Dependence of the cyclization of branched tetraethers on soil moisture in alkaline soils from arid-subhumid China: Implications for palaeorainfall reconstructions on the Chinese Loess Plateau. *Biogeosciences* **11**, 6755–6768.

Weijers J. W. H., Schouten S., van den Donker J. C., Hopmans E. C. and Sinninghe Damsté J. S. (2007) Environmental controls on bacterial tetraether membrane lipid distribution in soils. *Geochim. Cosmochim. Acta* **71**, 703–713.

Wulf H., Bookhagen B. and Scherler D. (2016) Differentiating between rain, snow, and glacier contributions to river discharge in the western Himalaya using remote-sensing data and distributed hydrological modeling. *Adv. Water Resour.* **88**, 1–81.

Wulf H., Bookhagen B. and Scherler D. (2010) Seasonal precipitation gradients and their impact on fluvial sediment flux in the Northwest Himalaya. *Geomorphology* **118**, 13–21.

Zech M., Zech R., Rozanski K., Gleixner G. and Zech W. (2015) Do n-alkane biomarkers in soils/sediments reflect the δ2H isotopic composition of precipitation? A case study from Mt. Kilimanjaro and implications for paleoaltimetry and paleoclimate research. *Isoopes Environ. Health Stud.* **51**, 508–524.

Zhisheng A., Kutzbach J. E., Prell W. L. and Porter S. C. (2001) Evolution of Asian monsoon and phased uplift of the Himalaya-Tibetan plateau since Late Miocene times. *Nature* **411**, 62–66.

Zhuang G., Brandon M. T., Pagani M. and Krishnan S. (2014) Leaf wax stable isotopes from Northern Tibetan Plateau: Implications for uplift and climate since 15 Ma. *Earth Planet. Sci. Lett.* **390**, 186–198.

Associate editor: Jessica Tierney